nature cell biology

aPKC phosphorylates NuMA-related LIN-5 to position the mitotic spindle during asymmetric division

Matilde Galli[1], Javier Muñoz[2,3], Vincent Portegijs[1], Mike Boxem[1], Stephan W. Grill[4,5], Albert J. R. Heck[2,3] and Sander van den Heuvel[1,6]

The position of the mitotic spindle controls the plane of cell cleavage and determines whether polarized cells divide symmetrically or asymmetrically[1–3]. In animals, an evolutionarily conserved pathway of LIN-5 (homologues: Mud and NuMA), GPR-1/2 (homologues: Pins, LGN, AGS-3) and Gα mediates spindle positioning, and acts downstream of the conserved PAR-3–PAR-6–aPKC polarity complex[1–6]. However, molecular interactions between polarity proteins and LIN-5–GPR–Gα remain to be identified. Here we describe a quantitative mass spectrometry approach for *in vivo* identification of protein kinase substrates. Applying this strategy to *Caenorhabditis elegans* embryos, we found that depletion of the polarity kinase PKC-3 results in markedly decreased levels of phosphorylation of a cluster of four LIN-5 serine residues. These residues are directly phosphorylated by PKC-3 *in vitro*. Phospho-LIN-5 co-localizes with PKC-3 at the anterior cell cortex and temporally coincides with a switch from anterior- to posterior-directed spindle movements in the one-cell embryo. LIN-5 mutations that prevent phosphorylation increase the extent of anterior-directed spindle movements, whereas phosphomimetic mutations decrease spindle migration. Our results indicate that anterior-located PKC-3 inhibits cortical microtubule pulling forces through direct phosphorylation of LIN-5. This molecular interaction between polarity and spindle-positioning proteins may be used broadly in cell cleavage plane determination.

The early *C. elegans* embryo provides a well-established model for studies of asymmetric cell division[3]. In this system, polarity proteins establish opposing cortical domains, in which the conserved PDZ-domain proteins PAR-3 (partitioning defective 3) and PAR-6 together with the PKC-3 atypical protein kinase C (aPKC) become restricted to the anterior cortex[7–10]. Simultaneously, the ring-finger protein PAR-2 occupies the posterior cortex together with the serine/threonine kinase PAR-1 (refs 11–13). The anterior–posterior polarity directs asymmetric division of the zygote. This involves posterior-directed movement of the mitotic spindle, which instructs cell cleavage to generate a larger anterior and smaller posterior blastomere[3,14]. It is not known how polarity proteins signal to the spindle to achieve asymmetric cell cleavage. Previous research has revealed an essential and conserved spindle-positioning pathway that consists of LIN-5 (abnormal cell lineage 5), GPR-1/2 (G protein regulator 1 and 2) and the closely related GOA-1 (G protein α_o subunit) and GPA-16 proteins in *C. elegans*, Mud, Pins and Gα in *Drosophila* and NuMA, the paralogues LGN and AGS-3 and Gα in mammals[4–6,15–20]. It is thought that LIN-5–GPR–Gα forms a cortical anchor for the minus-end-directed microtubule motor dynein, which in combination with microtubule depolymerization generates pulling forces that act from the cortex on astral microtubules[16]. Although it has been established that cell polarity creates asymmetry in the cortical pulling forces[14], a direct molecular connection between polarity determinants and the LIN-5–GPR–Gα complex is missing.

As the PKC-3 and PAR-1 protein kinases are major determinants of anterior and posterior polarity, we reasoned that these kinases may directly phosphorylate LIN-5–GPR–Gα to control spindle positioning. To investigate this possibility, we first examined whether the LIN-5–GPR–Gα complex is phosphorylated during asymmetric cell division. Immunoprecipitation of the LIN-5 complex from *C. elegans* embryo lysates followed by mass spectrometry revealed extensive levels of phosphorylation of LIN-5 at 25 different residues (Fig. 1a and Supplementary Tables S1 and S2). Next, we examined whether the polarity kinases PKC-3 or PAR-1 control LIN-5 phosphorylation *in vivo*. Hereto, we developed an approach that combines kinase inactivation, protein purification and quantitative mass spectrometry. This strategy makes use of differential metabolic labelling of *C. elegans* with stable ^{15}N or ^{14}N isotopes[21] (Fig. 1b; see Methods section). ^{15}N-labelled

[1]Developmental Biology, Utrecht University, 3584 CH Utrecht, The Netherlands. [2]Biomolecular Mass Spectrometry and Proteomics Group, Bijvoet Center for Biomolecular Research and Utrecht Institute for Pharmaceutical Sciences, Utrecht University, 3584 CH Utrecht, The Netherlands. [3]Netherlands Proteomics Center, The Netherlands. [4]Max Planck Institute of Molecular Cell Biology and Genetics, 01307 Dresden, Germany. [5]Max Planck Institute for the Physics of Complex Systems, 01187 Dresden, Germany.
[6]Correspondence should be addressed to S.v.d.H. (e-mail: S.J.L.vandenHeuvel@uu.nl)

Received 16 February 2011; accepted 5 July 2011; published online 21 August 2011; DOI: 10.1038/ncb2315

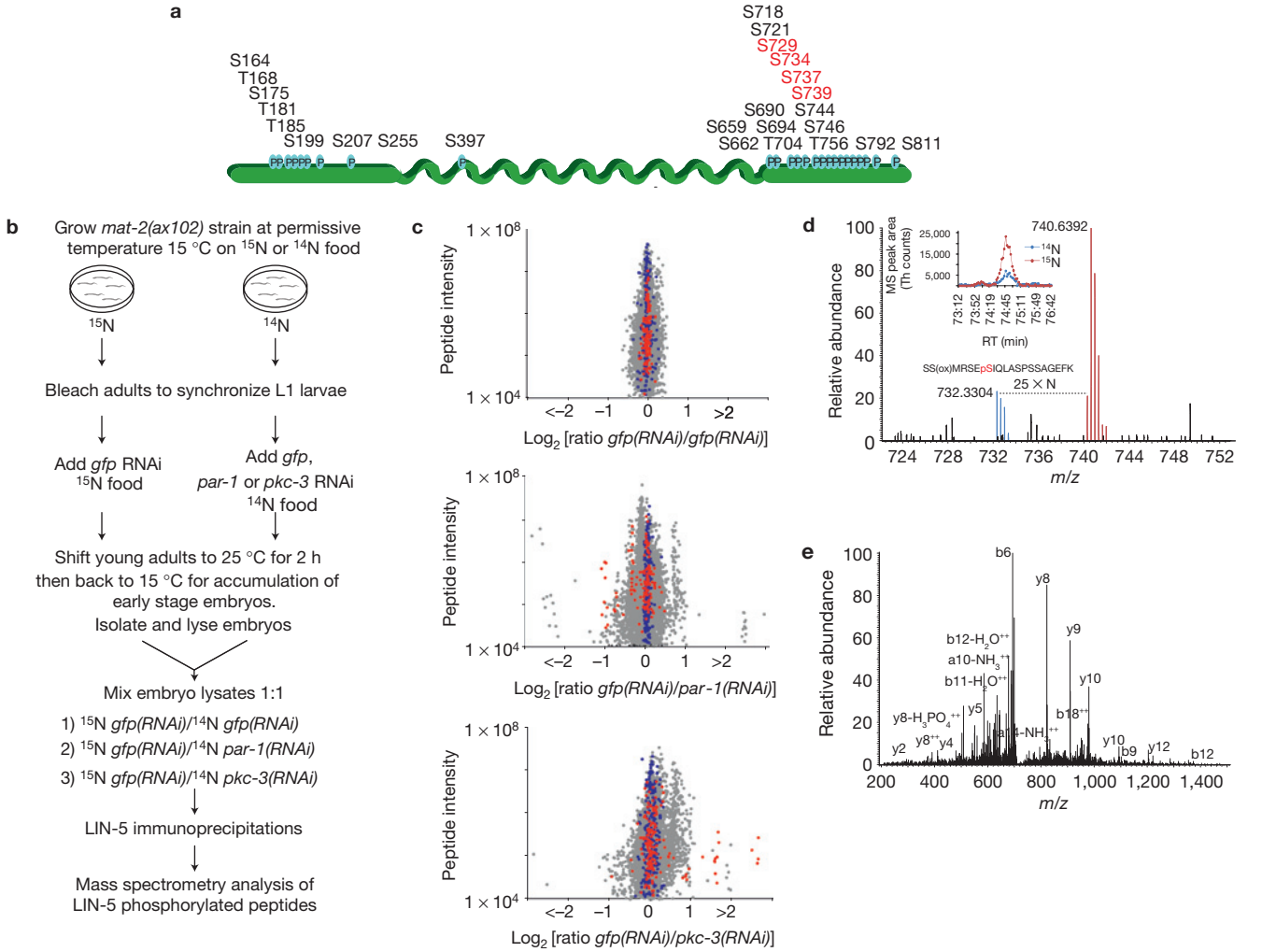

Figure 1 PKC-3 aPKC directs LIN-5 phosphorylation *in vivo*. (**a**) Analysis of LIN-5 immunoprecipitations from embryo lysates by tandem mass spectrometry revealed 25 phosphorylated residues. (**b**) Schematic overview of the quantitative mass spectrometry approach to determine whether LIN-5 phosphorylation is controlled by PKC-3 and PAR-1. (**c**) Log_2 ratios for all of the quantified $^{15}N/^{14}N$ peptide pairs as a function of their mass spectrometry intensities in the three LIN-5 immunoprecipitates. LIN-5 phosphopeptides are represented in red, and LIN-5 regular peptides are represented in blue. Peptides belonging to other proteins are shown in grey. Peptide intensities were calculated using the average of the ^{14}N and ^{15}N extracted ion chromatograms. (**d**) Example of a downregulated LIN-5 phosphopeptide in the ^{14}N *pkc-3(RNAi)*/^{15}N *gfp(RNAi)* experiment. Both precursor ions are shown, in blue (^{14}N) and red (^{15}N) colours (25 nitrogen atoms of mass difference). The inset shows the corresponding extracted-ion chromatograms for both species. MS, mass spectrometric, RT, retention time. Th, Thomson (unit of mass-to-charge ratio). (**e**) Annotated tandem mass spectrometry spectrum resulting from the collision-induced dissociation fragmentation of the ^{14}N peptide, indicating the presence of a phosphorylated Ser 737 residue. Additional information including post-translational modification scores can be found in Supplementary Tables S1 and S2.

cultures were treated with control *gfp* (green fluorescent protein) RNA interference (RNAi), and ^{14}N-labelled cultures were treated with either control *gfp* RNAi, RNAi of *pkc-3* or RNAi of *par-1*. Total embryonic protein lysates of these ^{15}N and ^{14}N cultures were mixed 1:1, followed by LIN-5 immunoprecipitation and analysis by mass spectrometry (Fig. 1b and Supplementary Table S1 and S2).

Control experiments in which ^{15}N and ^{14}N embryos were both treated with *gfp* RNAi showed equal amounts of LIN-5 (phospho)-peptides (Fig. 1c, top, and Supplementary Table S1 and S2). This demonstrates reliability of our quantitative mass spectrometry approach. Depletion of PAR-1 kinase did not cause a decrease in the level of any LIN-5 phosphopeptides. In fact, loss of PAR-1 resulted in an increase in the level of phosphorylation of five residues, demonstrating an indirect effect of *par-1(RNAi)* on LIN-5 phosphorylation (Fig. 1c, middle, and Supplementary Table S1). In contrast, knockdown of PKC-3 by RNAi resulted in a marked decrease in the levels of specific LIN-5 phosphopeptides (Fig. 1c, bottom, d and e). These peptides all contained the phosphorylated residues Ser 729, Ser 734, Ser 737 and/or Ser 739 in the carboxy terminus of LIN-5, whereas phosphorylation levels of other sites remained unaffected (Fig. 1c, bottom, and Supplementary Table S1). These results indicate that PKC-3 promotes phosphorylation of LIN-5 *in vivo*.

To determine whether PKC-3 phosphorylates LIN-5 directly, we carried out *in vitro* kinase assays. PKC-3, purified from embryo extracts through co-immunoprecipitation with GFP–PAR-6, was incubated with [γ-^{32}P]ATP and either glutathione *S*-transferase (GST)

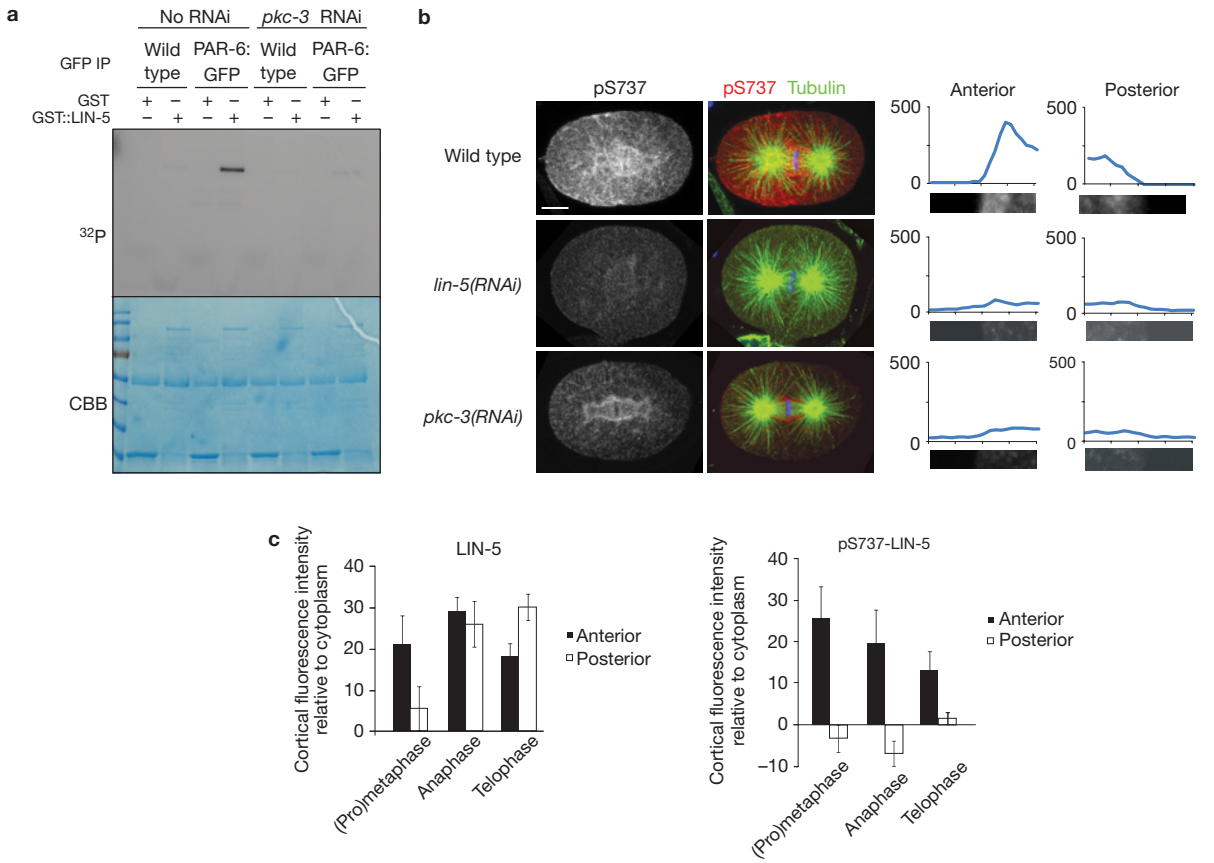

Figure 2 PKC-3 phosphorylates LIN-5 at the anterior cortex of the one-cell embryo. (**a**) *In vitro* kinase assay with recombinant GST–LIN-5 and GFP immunoprecipitations (IP) from control (wild type) embryos or embryos expressing PAR-6::GFP, treated with or without *pkc-3* RNAi. Top, autoradiogram; bottom, Coomassie brilliant blue (CBB)-stained gel. (**b**) Fluoresence micrographs, images of wild-type, *lin-5(RNAi)* and *pkc-3(RNAi) C. elegans* embryos at metaphase of the first division stained with anti-pS737 LIN-5 antibody (red) and anti-tubulin (green). Scale bar, 10 μm. The images on the right show a cortical region at higher magnification and an intensity plot of pS737 staining at the anterior versus posterior. (**c**) Quantification of cortical enrichment (relative to cytoplasm) of total LIN-5 (left) and LIN-5 pS737 (right) at different stages of mitosis: prometaphase/metaphase (LIN-5, $n=6$; pS737, $n=11$), anaphase (LIN-5, $n=13$; pS737, $n=7$) and telophase (LIN-5, $n=12$; pS737, $n=2$). See also Supplementary Figs S2 and S3. Error bars, s.e.m. at the 95% confidence level.

or GST–LIN-5. This resulted in a high level of phosphorylation of GST–LIN-5, but not of GST alone (Fig. 2a). RNAi of *pkc-3* prevented GST–LIN-5 phosphorylation; thus, a contaminating kinase is probably not responsible. We analysed *in vitro* phosphorylated GST–LIN-5 by mass spectrometry to determine which residues of LIN-5 are phosphorylated *in vitro*. This revealed exclusive phosphorylation of LIN-5 peptides containing Ser 729, Ser 734, Ser 737 and Ser 739, the same residues as identified in our *in vivo* quantitative mass spectrometry approach (Supplementary Fig. S1a). Moreover, mutation of the four serines to unphosphorylatable alanines resulted in a loss of LIN-5 phosphorylation *in vitro* (Supplementary Fig. S1b). Taken together, these results show that PKC-3 directly phosphorylates LIN-5 on four residues during asymmetric division.

To examine spatio-temporal control of LIN-5 phosphorylation by *pkc-3*, we generated antibodies against the phospho-S737 LIN-5 peptide (corresponding to the site most strongly downregulated after *pkc-3* RNAi). These antibodies were phospho-LIN-5 specific, as they recognized *in vitro* phosphorylated GST–LIN-5, but not unphosphorylatable GST–LIN-5 4A (a mutant in which the four serines were changed to alanine) in western blot experiments (Supplementary Fig. S1c). In immunofluorescence microscopy experiments, the anti-pS737-LIN-5 antibodies stained the cell cortex, nuclear envelope, spindle microtubules and cytoplasm of one-cell embryos (Figs 2b, 3a and Supplementary Fig. S2). Except for the nuclear envelope, this staining was LIN-5 specific, as it was almost completely absent in *lin-5* RNAi embryos (Fig. 2b and Supplementary Fig. S2a).

Importantly, the level of pS737 staining was substantially enriched at the anterior cortex, compared with the posterior cortex, throughout cell division (Fig. 2b, quantified in Fig. 2c, right; see also Fig. 3a and Supplementary Fig. S2). In contrast, staining with monoclonal antibodies revealed that the total pool of LIN-5 was enriched at the anterior cortex during early mitosis, but gradually became more abundant at the posterior cortex (Fig. 2c, left, and Supplementary Fig. S3). Consistent with anterior pS737-LIN-5 enrichment, PKC-3 localizes specifically to the anterior cortex and cytoplasm[9]. RNAi of *pkc-3* strongly decreased the level of pS737 staining, demonstrating that PKC-3 spatially controls the phosphorylation of LIN-5 Ser 737 in the one-cell embryo (Fig. 2b and Supplementary Fig. S2b). We examined whether LIN-5 Ser 737 phosphorylation depends on PAR asymmetry and cortical localization of PKC-3. The cortical domain

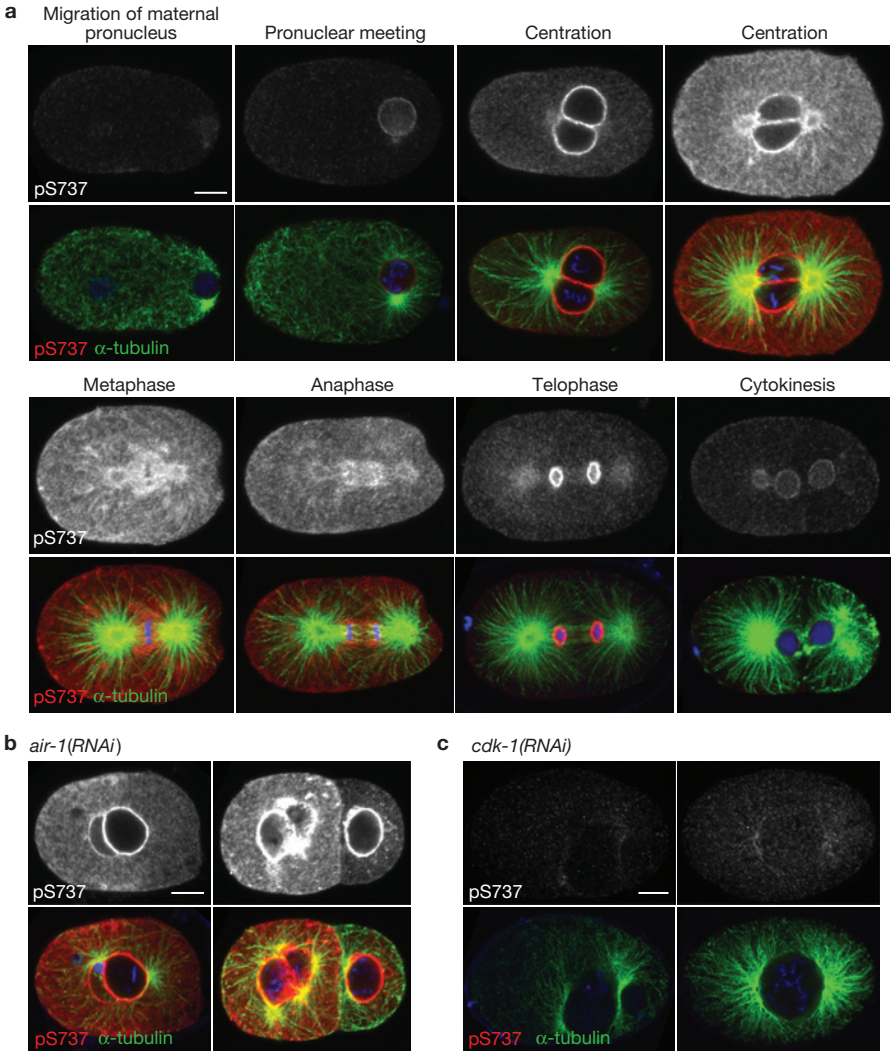

Figure 3 PKC-3 phosphorylates LIN-5 in mitosis and requires CDK-1. One-cell embryos at different stages after pronuclear migration immunostained for pS737-LIN-5 (red) and α-tubulin (green). (**a**) Wild-type embryos. (**b**) *air-1(RNAi)* embryos. (**c**) *cdk-1(RNAi)* embryos. Scale bars, 10 μm.

of pS737-LIN-5 expanded more posteriorly in *par-2* RNAi embryos, which is consistent with the expansion of cortical PKC-3 in *par-2* mutants[9] (Supplementary Fig. S4, white arrowheads). In *par-6* RNAi embryos, the level of pS737-LIN-5 staining was strongly decreased at the cortex but not in the cytoplasm (Supplementary Fig. S4, open arrowheads). This is in agreement with PAR-6 requirement in cortical PKC-3 localization[9], and demonstrates that PKC-3 does not need to be associated with PAR-6 to phosphorylate LIN-5 in the cytoplasm. Together, these observations indicate that asymmetrically localized PKC-3 phosphorylates LIN-5 at the anterior cortex and cytoplasm of the one-cell embryo.

Next, we carried out a detailed temporal analysis of pS737 staining (Fig. 3a and Supplementary Fig. S2). Cortical pS737 staining first became detectable in the one-cell embryo when the female pronucleus migrates towards the male pronucleus, and increased during the subsequent movement of the united pronuclei to the middle of the cell (Fig. 3a and Supplementary Fig. S2). The latter centration process occurs during mitotic prophase and depends on cortical pulling forces[22,23]. The level of pS737-LIN-5 staining was highest from the time of late prophase and throughout metaphase, started to decline in late anaphase and was largely gone by telophase/cytokinesis.

Owing to the strong increase of pS737 staining during prophase–metaphase, we speculated that a cell-cycle-dependent signal may trigger the phosphorylation of LIN-5 by PKC-3. In *Drosophila*, Aurora A kinase activates aPKC to direct the asymmetric localization of LGL in dividing neural progenitors[24]. *C. elegans* AIR-1 Aurora A did not seem to be needed for PKC-3 C-mediated phosphorylation of LIN-5, as the level of pS737 staining was not diminished in *air-1* RNAi embryos (Fig. 3b). However, depletion of the core cell-cycle kinase CDK-1 resulted in a complete loss of pS737 staining (Fig. 3c). As Ser 737 is not phosphorylated by CDK1 *in vitro* (unpublished results), it is likely that CDK-1 either functions to activate PKC-3 in mitosis, or acts as a priming kinase for LIN-5 phosphorylation by PKC-3. Taken together, these results show that LIN-5 is phosphorylated by PKC-3 during the processes of pronuclear centration and spindle positioning, that this phosphorylation occurs asymmetrically at the anterior cell cortex, in agreement with the

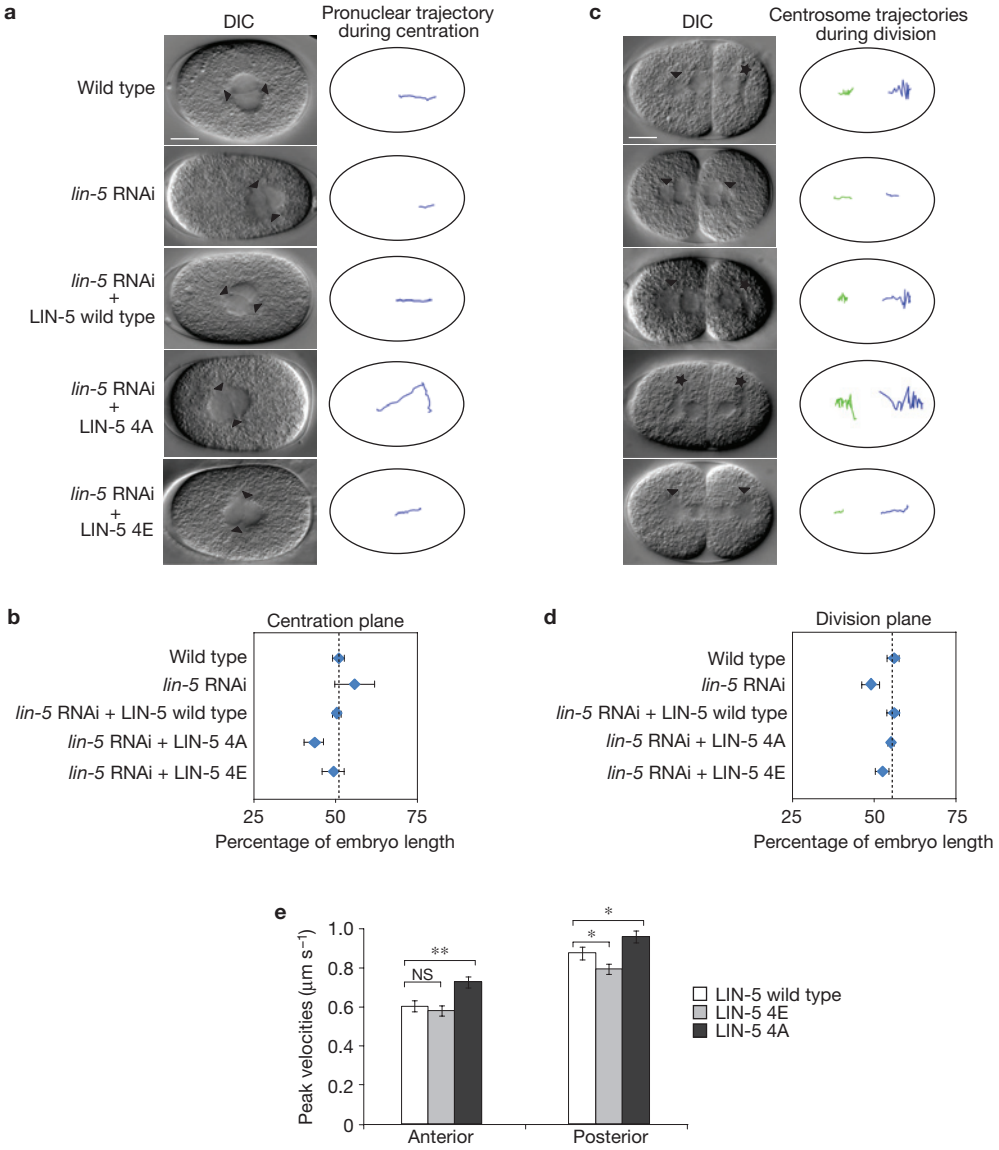

Figure 4 PKC-3-mediated phosphorylation of LIN-5 directs mitotic spindle positioning in the one-cell embryo. (**a**) Pronuclear centration in wild-type, *lin-5(RNAi)* or *lin-5* phospho-mutant embryos treated with *lin-5* RNAi to deplete endogenous LIN-5. DIC images are taken just before NEB. The arrowheads indicate the centrosome position. The right panels show trajectories of pronuclei from pronuclear meeting to NEB. Scale bar, 10 μm. (**b**) Quantification of the extent of centration, with the average position indicated as a percentage of embryo length (0% anterior and 100% posterior) and the standard deviation (wild type, $n = 10$; *lin-5* RNAi, $n = 12$; *lin-5* RNAi + LIN-5 wild type, $n = 15$; *lin-5* RNAi + LIN-5 4A, $n = 7$; *lin-5* RNAi + LIN-5 4E, $n = 9$). The dotted line shows the average position of centration in wild-type embryos. (**c**) Spindle movements during division in wild-type, *lin-5(RNAi)* or *lin-5* phospho-mutant embryos treated with *lin-5* RNAi to deplete endogenous LIN-5. DIC images were taken just after completion of the first division. The arrowheads indicate a round anterior centrosome; the asterisks represent the flattened posterior centrosome. Note that in LIN-5 4A mutants both centrosomes are flattened, whereas in LIN-5 4E mutants both centrosomes are round. The right panels show centrosome trajectories of embryos from NEB to completion of cytokinesis. Scale bar, 10 μm. (**d**) Quantification of the cleavage plane in different embryos, with the average position indicated as a percentage of embryo length (0% anterior and 100% posterior) and the standard deviation (wild type, $n = 10$; *lin-5* RNAi, $n = 12$; *lin-5* RNAi + LIN-5 wild type, $n = 15$; *lin-5* RNAi + LIN-5 4A, $n = 7$; *lin-5* RNAi + LIN-5 4E, $n = 9$). The dotted line shows the average position of cleavage in wild-type embryos. (**e**) Mean peak velocities (μm s^{-1}) of anterior and posterior spindle poles measured in a 10 s time frame after spindle severing in one-cell embryos of the indicated genotypes. Error bars, s.e.m. $^{*}P < 0.05$ when compared with wild type, $^{**}P < 0.01$ when compared with wild type, NS not significant.

localization of PKC-3, and that this phosphorylation is tightly coupled to cell-cycle progression.

Next, we investigated the functional relevance of LIN-5 phosphorylation by PKC-3 *in vivo*. We generated an unphosphorylatable LIN-5 mutant, in which the four serines were changed to alanine (4A), as well as a phosphomimetic mutant, in which the four serines were mutated to glutamic acid (4E). For a reliable comparison between mutant and wild-type LIN-5, we used homologous recombination with the MosSCI (Mos1-mediated single-copy insertion) technique to generate transgenic strains[25]. This allowed single-copy integration of *lin-5* wild-type, *lin-5* 4A and *lin-5* 4E transgenes at an identical position of chromosome IV. Each of these transgenes included a large

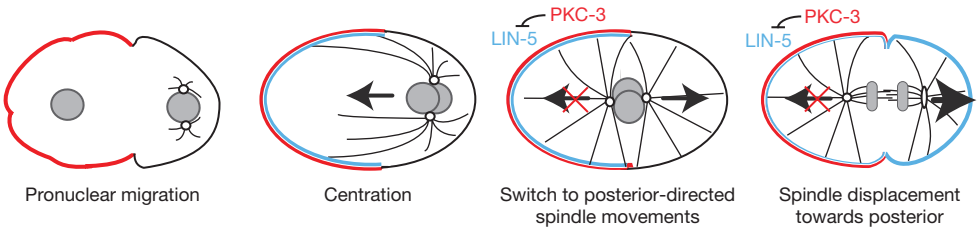

Figure 5 Model illustrating how phosphorylation of LIN-5 by PKC-3 may control the position of the mitotic spindle in the one-cell embryo. Phosphorylation of LIN-5 (blue) by PKC-3 (red) begins during pronuclear centration and proceeds until anaphase. Phosphorylation inhibits cortical microtubule pulling forces at the anterior cortex, allowing the spindle to switch from anterior-directed movements during centration to posterior-directed movements during metaphase and anaphase.

number of silent mutations in the first 377 nucleotides of the *lin-5* coding sequences, to allow knockdown of endogenous *lin-5* by RNAi without inhibition of the *lin-5* transgene.

We examined whether mutation of the *lin-5* phosphorylation sites affected movements of the pronuclei and spindle in the one-cell embryo. After fertilization of a wild-type oocyte, the maternal nucleus completes meiosis in the anterior and then migrates to the paternal pronucleus in the posterior. Together, the two pronuclei migrate back to the middle of the zygote during centration and rotation, followed by nuclear envelope breakdown (NEB) and chromosome alignment in the centre (Fig. 4a,b). Next, the mitotic spindle is pulled towards the posterior during metaphase/anaphase and the zygote divides at roughly 55% of the cell length, resulting in a larger anterior AB daughter cell and a smaller posterior P1 cell (Fig. 4c,d). Both centration of the pronuclei and posterior displacement of the mitotic spindle depend on cortical microtubule pulling forces generated by the LIN-5–GPR–Gα complex[4,22,26,27].

After *lin-5* RNAi, the pronuclei centrate slowly to the middle and are still in the posterior at the time of NEB (Fig. 4a,b), indicative of a loss of cortical pulling forces[23,27]. Moreover, the mitotic spindle is not pulled towards the posterior during anaphase and the cell divides symmetrically, or even forms a smaller AB cell[4,26] (Fig. 4c,d). Strikingly, in embryos expressing unphosphorylatable LIN-5 4A, the pronuclei moved further to the anterior during centration than in the wild-type embryos (43.7 ± 2.8% versus 51.6 ± 1.3% of embryo length, respectively, $P = 0.00008$; Fig. 4a,b). Similarly to LIN-5 4A mutants, *pkc-3(RNAi)* embryos showed overcentration of the nucleo-centrosomal complex (Supplementary Fig. S5). During division, some *lin-5* 4A embryos showed exaggerated rocking movements and flattening of the anterior centrosome (Fig. 4c), resembling the normal behaviour of the posterior centrosome. To determine whether phosphorylation of LIN-5 by PKC-3 affected cortical microtubule pulling forces during anaphase, we measured the peak velocities of the spindle poles after laser ablation of the spindle midzone at the beginning of anaphase. In LIN-5 4A mutants, we found a 21% increase in anterior spindle pole velocities, compared with wild-type LIN-5 (0.73 ± 0.028 μm s^{-1} (mean ± s.e.m.), $n = 26$, versus 0.60 ± 0.027 μm s^{-1}, $n = 40$, respectively, $P = 0.0018$; Fig. 4e and Supplementary Fig. S6). Most *lin-5* 4A embryos achieved an asymmetric spindle position in late mitosis, unlike *pkc-3(RNAi)* embryos, which divide symmetrically[9] (Fig. 4c,d and Supplementary Fig. S5). These results indicate that PKC-3 inhibits cortical pulling forces in part through LIN-5 phosphorylation, probably in combination with other factors, such as PAR-1, PAR-2, LET-99 and PPK-1, that become posteriorly displaced in a PKC-3-dependent manner[9,28–30].

Embryos depleted of endogenous LIN-5 and reconstituted with phosphomimetic LIN-5 4E showed normal centration, but completely lacked spindle rocking and largely failed to displace the spindle towards the posterior after NEB, resulting in a more symmetric division than wild-type embryos (52.2 ± 2.1% versus 55.4 ± 1.0% of embryo length, respectively, $P = 0.005$; Fig. 4c,d). Spindle ablation experiments revealed that in LIN-5 4E mutants, the speed of the movements of the posterior pole was decreased by 9% when compared with the posterior pole in the presence of wild-type LIN-5 (0.79 ± 0.028 μm s^{-1}, $n = 32$, versus 0.87 ± 0.033 μm s^{-1}, $n = 40$, respectively, $P = 0.038$; Fig. 4e). Furthermore, expression of the LIN-5 4E mutant caused defects in meiosis (data not shown), similar to the defects in *lin-5* RNAi embryos[15,22]. Thus, specific mutations that mimic the PKC-3 phosphorylation of LIN-5 cause partial LIN-5 loss-of-function. Together, these results indicate that PKC-3 phosphorylates LIN-5 to negatively regulate the cortical microtubule pulling forces at the anterior cortex during asymmetric division of the one-cell embryo (Fig. 5).

To determine whether the phosphorylation of LIN-5 controls its localization in the cell, we analysed the localization of the LIN-5 4A and 4E mutants. The LIN-5 4A and 4E proteins localize to the cell cortex and to the spindle poles, similar to the localization of the normal protein (Supplementary Fig. S7). Thus, phosphorylation of LIN-5 does not seem to be critical in protein localization. Furthermore, the interaction between LIN-5 and GPR-1/2, and the localization of GPR-1/2, were not affected by the LIN-5 phosphorylation-site mutations (Supplementary Fig. S7a,b). However, the protein levels of the LIN-5 4E mutant were decreased when compared with the normal protein (Supplementary Fig. S7b), which was confirmed in three independently integrated LIN-5 4E mutant strains (data not shown). Together these results show that PKC-3 phosphorylation does not affect the localization of LIN-5 or its association with GPR-1/2. It will be interesting to determine whether PKC-3 phosphorylation of LIN-5 affects interactions with other binding partners, dynamics of LIN-5 complexes, LIN-5 protein turnover or the function of another complex such as dynein.

Here, we have applied a combined kinase knockdown/quantitative mass spectrometry approach of early *C. elegans* embryos to determine how polarity proteins control spindle positioning during asymmetric division. Our results support a model in which anteriorly localized PKC-3 phosphorylates LIN-5 in late prophase to inhibit the anterior-directed movement of the nucleo-centrosomal complex and to promote higher net cortical pulling forces in the posterior. This results in

posterior spindle migration and asymmetric cell cleavage (Fig. 5). Interestingly, aPKC has recently also been shown to phosphorylate the mammalian GPR-1/2 homologue Pins, thereby directing spindle orientation in polarized tissue culture cells[31]. A crucial process such as spindle positioning is probably controlled by multiple parallel pathways, as is highlighted by correction of the mispositioned spindle during late division of LIN-5 4A embryos. The aPKC complex and LIN-5–GPR–Gα complex are common regulators of polarity and spindle positioning in metazoans. Hence, the discovered direct link between cell polarity and the spindle-positioning machinery may provide a conserved mechanism for positioning the spindle in polarized cells, for instance to promote cell cleavage within the plane of an epithelium. □

METHODS

Methods and any associated references are available in the online version of the paper at http://www.nature.com/naturecellbiology

Note: Supplementary Information is available on the Nature Cell Biology website

ACKNOWLEDGEMENTS

We thank J. Krijgsveld for help in the initial phases of the project, and A. Thomas and M. Tanenbaum for critically reading the manuscript, helpful advice and support throughout the project. We thank members of the van den Heuvel and Boxem laboratories for fruitful discussions. We are grateful to C. Frokjaer-Jensen and E. Jorgensen for reagents and advice on MosSCI. M.G. was supported by a predoctoral fellowship from the Boehringer Ingelheim Fonds and foundation 'De Drie Lichten' in the Netherlands. This work was also supported by the Netherlands Proteomics Centre, which is part of the Netherlands Genomics Initiative.

AUTHOR CONTRIBUTIONS

M.G. and S.v.d.H. designed the project and wrote the manuscript. J.M. and A.J.R.H. helped design the quantitative mass spectrometry experiments, J.M. carried out the mass spectrometry experiments and analysed the data. M.G. carried out all other experiments. V.P. and M.B. provided help in molecular cloning and yeast two-hybrid experiments. S.W.G. guided the spindle severing experiments. All authors discussed the results and commented on the manuscript.

COMPETING FINANCIAL INTERESTS

The authors declare no competing financial interests.

Published online at http://www.nature.com/naturecellbiology
Reprints and permissions information is available online at http://www.nature.com/reprints

1. Knoblich, J. A. Asymmetric cell division: recent developments and their implications for tumour biology. *Nat. Rev. Mol. Cell Biol.* **11,** 849–860 (2010).
2. Siller, K. H. & Doe, C. Q. Spindle orientation during asymmetric cell division. *Nat. Cell Biol.* **11,** 365–374 (2009).
3. Galli, M. & van den Heuvel, S. Determination of the cleavage plane in early *C. elegans* embryos. *Annu. Rev. Genet.* **42,** 389–411 (2008).
4. Srinivasan, D. G., Fisk, R. M., Xu, H. & van den Heuvel, S. A complex of LIN-5 and GPR proteins regulates G protein signaling and spindle function in *C. elegans*. *Genes Dev.* **17,** 1225–1239 (2003).
5. Colombo, K. *et al.* Translation of polarity cues into asymmetric spindle positioning in *Caenorhabditis elegans* embryos. *Science* **300,** 1957–1961 (2003).
6. Gotta, M. *et al.* Asymmetrically distributed *C. elegans* homologs of AGS3/PINS control spindle position in the early embryo. *Curr. Biol.* **13,** 1029–1037 (2003).
7. Etemad-Moghadam, B., Guo, S. & Kemphues, K. J. Asymmetrically distributed PAR-3 protein contributes to cell polarity and spindle alignment in early *C. elegans* embryos. *Cell* **83,** 743–752 (1995).
8. Hung, T. J. & Kemphues, K. J. PAR-6 is a conserved PDZ domain-containing protein that colocalizes with PAR-3 in *Caenorhabditis elegans* embryos. *Development* **126,** 127–135 (1999).
9. Tabuse, Y. *et al.* Atypical protein kinase C cooperates with PAR-3 to establish embryonic polarity in *Caenorhabditis elegans*. *Development* **125,** 3607–3614 (1998).
10. Cuenca, A. A. *et al.* Polarization of the *C. elegans* zygote proceeds via distinct establishment and maintenance phases. *Development* **130,** 1255–1265 (2003).
11. Boyd, L. *et al.* PAR-2 is asymmetrically distributed and promotes association of P granules and PAR-1 with the cortex in *C. elegans* embryos. *Development* **122,** 3075–3084 (1996).
12. Guo, S. & Kemphues, K. J. par-1, a gene required for establishing polarity in *C. elegans* embryos, encodes a putative Ser/Thr kinase that is asymmetrically distributed. *Cell* **81,** 611–620 (1995).
13. Hao, Y., Boyd, L. & Seydoux, G. Stabilization of cell polarity by the *C. elegans* RING protein PAR-2. *Dev. Cell* **10,** 199–208 (2006).
14. Grill, S. W., Gonczy, P., Stelzer, E. H. & Hyman, A. A. Polarity controls forces governing asymmetric spindle positioning in the *Caenorhabditis elegans* embryo. *Nature* **409,** 630–633 (2001).
15. van der Voet, M. *et al.* NuMA-related LIN-5, ASPM-1, calmodulin and dynein promote meiotic spindle rotation independently of cortical LIN-5/GPR/Gα. *Nat. Cell Biol.* **11,** 269–277 (2009).
16. Nguyen-Ngoc, T., Afshar, K. & Gonczy, P. Coupling of cortical dynein and Gα proteins mediates spindle positioning in *Caenorhabditis elegans*. *Nat. Cell Biol.* **9,** 1294–1302 (2007).
17. Bowman, S. K. *et al.* The *Drosophila* NuMA homolog Mud regulates spindle orientation in asymmetric cell division. *Dev. Cell* **10,** 731–742 (2006).
18. Du, Q. & Macara, I. G. Mammalian Pins is a conformational switch that links NuMA to heterotrimeric G proteins. *Cell* **119,** 503–516 (2004).
19. Izumi, Y. *et al.* *Drosophila* Pins-binding protein Mud regulates spindle-polarity coupling and centrosome organization. *Nat. Cell Biol.* **8,** 586–593 (2006).
20. Siller, K. H., Cabernard, C. & Doe, C. Q. The NuMA-related Mud protein binds Pins and regulates spindle orientation in *Drosophila* neuroblasts. *Nat. Cell Biol.* **8,** 594–600 (2006).
21. Krijgsveld, J. *et al.* Metabolic labeling of *C. elegans* and *D. melanogaster* for quantitative proteomics. *Nat. Biotechnol.* **21,** 927–931 (2003).
22. Goulding, M. B. *et al.* Control of nuclear centration in the *C. elegans* zygote by receptor-independent Gα signaling and myosin II. *J. Cell Biol.* **178,** 1177–1191 (2007).
23. Labbe, J. C., McCarthy, E. K. & Goldstein, B. The forces that position a mitotic spindle asymmetrically are tethered until after the time of spindle assembly. *J. Cell Biol.* **167,** 245–256 (2004).
24. Wirtz-Peitz, F., Nishimura, T. & Knoblich, J. A. Linking cell cycle to asymmetric division: Aurora-A phosphorylates the Par complex to regulate Numb localization. *Cell* **135,** 161–173 (2008).
25. Frokjaer-Jensen, C. *et al.* Single-copy insertion of transgenes in *Caenorhabditis elegans*. *Nat. Genet.* **40,** 1375–1383 (2008).
26. Lorson, M. A., Horvitz, H. R. & van den Heuvel, S. LIN-5 is a novel component of the spindle apparatus required for chromosome segregation and cleavage plane specification in *Caenorhabditis elegans*. *J. Cell Biol.* **148,** 73–86 (2000).
27. Park, D. H. & Rose, L. S. Dynamic localization of LIN-5 and GPR-1/2 to cortical force generation domains during spindle positioning. *Dev. Biol.* **315,** 42–54 (2008).
28. Panbianco, C. *et al.* A casein kinase 1 and PAR proteins regulate asymmetry of a PIP(2) synthesis enzyme for asymmetric spindle positioning. *Dev. Cell* **15,** 198–208 (2008).
29. Rose, L. S. & Kemphues, K. The let-99 gene is required for proper spindle orientation during cleavage of the *C. elegans* embryo. *Development* **125,** 1337–1346 (1998).
30. Krueger, L. E., Wu, J. C., Tsou, M. F. & Rose, L. S. LET-99 inhibits lateral posterior pulling forces during asymmetric spindle elongation in *C. elegans* embryos. *J. Cell Biol.* **189,** 481–495 (2010).
31. Hao, Y. *et al.* Par3 controls epithelial spindle orientation by aPKC-mediated phosphorylation of apical Pins. *Curr. Biol.* **20,** 1809–1818 (2010).

METHODS

Molecular cloning. For MosSCI integration on chromosome IV, *Ppie-1::lin-5 synthetic 377::pie-1 3′UTR* was generated by amplifying the 130-base-pair (bp) *pie-1* 3′ UTR from genomic N2 DNA using KOD Hot Start DNA Polymerase (Novagen) and cloning it into the pCFJ178 vector (a gift from E. Jorgensen, HHMI, University of Utah, USA). Subsequently, a 1.1-kilobase *pie-1* promoter sequence was PCR amplified with KOD from genomic N2 DNA and inserted. The first 377 coding nucleotides of genomic *lin-5* were replaced by a codon-altered sequence to resist RNAi before inserting it in between the promoter and 3′ UTR. For yeast two-hybrid analysis, the *gpr-1* open reading frame was PCR amplified using KOD polymerase from a full-length *gpr-1* Gateway entry clone[32], and cloned in frame with the Gal4 DNA binding domain (DB) into vector pMB34 (a modified pPC97 vector[33] that includes the CAN1 gene and places a 3×glycine linker between the DB and the insert; sequence available on request). *lin-5* coding sequence fragments (Supplementary Fig. S3b) were PCR amplified using KOD polymerase from a full-length *lin-5* Gateway entry clone[34], and cloned in frame with the Gal4 activation domain (AD) in vector pPC86-AN, using AscI and NotI (ref. 32).

Strains and culture. Worms were cultured on NGM plates seeded with OP50 bacteria. The strains used in this study can be found in Supplementary Table S4 (refs 35,36). All strains were maintained at 20 °C, except DS98 (ref. 35), which was maintained at 15 °C.

Isotopic labelling of *C. elegans*. For the quantitative mass spectrometry experiments, *mat-2(ax102)* worms were grown at 15 °C on agarose plates containing 1.2% agarose, 50 mM NaCl, 5 μg ml^{-1} cholesterol, 1 mM $CaCl_2$, 1 mM $MgCl_2$ and 25 mM K_2HPO_4/KH_2PO_4, at pH 6.0, and 1/5 final volume of 98% ^{15}N-enriched medium or unlabelled medium (Spectra 9-^{15}N or Spectra 9-Unlabelled, Cambridge Isotope laboratories) and seeded with a ten times concentrated overnight culture of HB101 bacteria grown in either Spectra 9-^{15}N or Spectra 9-Unlabelled medium. The next generation of worms were bleached and embryos were allowed to hatch in S-medium and divided into six liquid cultures, three ^{15}N cultures and three ^{14}N cultures, each containing ∼750,000 L1 stage larvae. For the *par-1(RNAi)* culture, unlabelled *par-1* RNAi bacteria were added to one of the ^{14}N *mat-2(ax102)* L1 cultures and were grown for ∼120 h at 15 °C. For the *pkc-3(RNAi)* culture, a ^{14}N *mat-2(ax102)* culture was first grown with unlabelled NA22 bacteria for 68 h, then the worms were washed twice with fresh S-medium and unlabelled *pkc-3* RNAi bacteria was added to the cultures and grown for a further 25 h at 15 °C. As a control for the *pkc-3(RNAi)* culture, one of the ^{15}N *mat-2(ax102)* cultures was first grown with ^{15}N-labelled NA22 bacteria for 68 h, and then with ^{15}N-labelled *gfp* RNAi bacteria for 25 h. The other three *gfp(RNAi) mat-2(ax102)* cultures were grown with *gfp* RNAi bacteria from the L1 stage onward, two cultures with ^{15}N-labelled *gfp* RNAi bacteria and one with ^{14}N-labelled *gfp* RNAi bacteria. All cultures were individually monitored and shifted to 25 °C for two hours when most of the worms in the culture were very young adults to accumulate fertilized eggs in meiosis. The cultures were then cooled back to 15 °C and grown for a further 30 min. The gravid worms were then collected and embryos were isolated by hypochlorite treatment.

RNA-mediated interference. For the quantitative mass spectrometry experiment, bacteria expressing RNAi feeding vector for *gfp*, *pkc-3* or *par-1* were grown overnight in 98% ^{15}N-enriched medium or unlabelled medium (Spectra 9-^{15}N or Spectra 9-Unlabelled, Cambridge Isotope laboratories), and then for a further 6 h after the addition of 2 mM IPTG (isopropyl-β-D-thiogalactoside). For other RNAi experiments, either double-stranded RNA (dsRNA) was injected into the gonad of young adults (for *lin-5* and *pkc-3*) or L4 stage animals were put on RNAi feeding plates, for 48 h (*pkc-3*, *air-1*, *cdk-1*, *par-2* and *par-6*).

Embryo lysis and immunoprecipitations. Embryo pellets were snap frozen in liquid nitrogen, ground using a Mikro-Dismembrator (Sartorius, 30 s at a frequency of 1,500 min^{-1}) and resuspended in fresh lysis buffer (containing 20 mM Tris-HCl at pH 7.8, 250 mM NaCl, 15% glycerol, 1% Triton X-100, 0.5 mM EDTA, 1 mM β-mercaptoethanol, 10 mM 1-naphthyl phosphate monosodium salt monohydrate, 50 mM sodium fluoride, 10 mM sodium pyrophosphate decahydrate, 100 μM sodium orthovanadate and protease inhibitors (Roche complete, Mini, EDTA-free)). The lysate was cleared at 13,000 r.p.m. (14,000*g*) for 15 min at 4 °C in an Eppendorf microcentrifuge. The protein concentrations were then measured and ^{14}N and ^{15}N embryos were mixed at a 1:1 ratio. For the ^{15}N *gfp(RNAi)*/^{14}N *gfp(RNAi)* experiment, 15 mg of mixed protein lysate was used for the immunoprecipitations. For the ^{15}N *gfp(RNAi)*/^{14}N *par-1(RNAi)* and the ^{15}N *gfp(RNAi)*/^{14}N *pkc-3(RNAi)* experiments, 8.3 mg and 5.6 mg of protein lysate were used, respectively. Immunoprecipitations were carried out at 4 °C for 2 h with rabbit anti-LIN-5 antibodies covalently bound to protein A Sepharose beads, using 15 μl beads per milligram of lysate. The immunoprecipitated material was eluted with 400 μl 2*x* sample buffer lacking β-mercaptoethanol at 37 °C with shaking for 50 min. The sample was then dialysed against 1 mM Tris at pH 9.0, 0.01% SDS and 1 mM β-mercaptoethanol and concentrated by cold-trap speed vacuum centrifugation. Immunoprecipitated proteins were separated on 8% SDS polyacrylamide gels, fixed for 15 min in 25% isopropanol with 10% acetic acid and stained with Coomassie brilliant blue (Pageblue, Fermentas) for 1 h.

In-gel digestion and phosphopeptide enrichment. Gel bands were cut and processed for protein in-gel digestion. Briefly, proteins were reduced with dithiothreitol and then alkylated with iodoacetamide. Trypsin was added at a concentration of 10 ng μl^{-1} and digested overnight at 37 °C. Subsequently, peptides were collected from the supernatants and a second extraction using 10% formic acid was carried out. Phosphopeptides from LIN-5 were enriched using TiO_2 chromatography[37]. Basically, home-made GELoader tips (Eppendorf) were packed with TiO_2 beads (5 μm, INERTSIL). Peptides were loaded in 10% formic acid and subsequently washed with 20 μl of 80% acetonitrile with 0.1% trifluoroacetic acid (Fluka, Sigma-Aldrich). Phosphopeptides were then eluted twice with 20 μl of 1.25% ammonia solution (Merck), at pH 10.5, and 3 μl of 100% formic acid was finally added to acidify the samples.

Mass spectrometric analysis. Nanoflow liquid chromatography with tandem mass spectrometry was carried out by coupling an Agilent 1100 high-performance liquid chromatography system (Agilent Technologies) to an LTQ-Orbitrap XL mass spectrometer (Thermo Electron). Peptide samples were delivered to a trap column (AquaTM C18, 5 μm (Phenomenex); 20 mm × 100 μm inner diameter, packed in-house) at 5 μl min^{-1} in 100% solvent A (0.1 M acetic acid in water). Next, peptides were eluted from the trap column onto an analytical column (ReproSil-Pur C18-AQ, 3 μm, Dr. Maisch GmbH; 40 cm × 50 μm inner diameter, packed in-house) at ∼100 nl min^{-1} in a 90 min or 3 h gradient from 0 to 40% solvent B (0.1 M acetic acid in 8:2 (v/v) acetonitrile/water). The eluent was sprayed using distal coated emitter tips butt-connected to the analytical column. The mass spectrometer was operated in data-dependent mode, automatically switching between mass spectrometry and tandem mass spectrometry. Full-scan mass spectrometry spectra (from m/z 300 to 1,500) were acquired in the Orbitrap with a resolution of 60,000 at m/z 400 after accumulation to a target value of 500,000 in the linear ion trap. The five most intense ions at a threshold above 5,000 were selected for collision-induced fragmentation in the linear ion trap at a normalized collision energy of 35% after accumulation to a target value of 10,000.

Peptide analysis. Peak lists were created from raw files with MaxQuant[38]. Peptide identification was carried out with Mascot (Matrix Science) against a *C. elegans* protein database (http://www.wormbase.org) supplemented with all of the frequently observed contaminants in mass spectrometry (23,502 protein sequences in total). The following parameters were used: 10 ppm precursor mass tolerance, 0.6 Da fragment ion tolerance, up to three missed cleavages, carbamidomethyl cysteine as a fixed modification, oxidized methionine, and phosphorylated serine, threonine and tyrosine as variable modifications. A ^{15}N-based quantification method was used in Mascot, where a given peptide is set to carry one type of modification and never a mixture, to prevent any matches to peptides with mixed or partial labelling. Quantitative analysis of peptide doublets and post-translational modification scoring to assign the phosphorylation site within the sequence[39] were carried out using an in-house ^{15}N-adapted version of MSQuant software[40] and manually validated. Briefly, peptide ratios were determined using the extracted-ion chromatograms of the mono-isotopic peaks of the ^{14}N- and ^{15}N-labelled peptides. Peptides with poor signal-to-noise ratios, overlapping isotopic clusters or with interfering signals were rejected and were not used for the quantification. Peptide ratios were normalized by subtracting the median of the whole distribution ($\log_2$). The ratios of all of the identified proteins in the three immunoprecipitates were calculated as the arithmetic median of the peptide ratios (Supplementary Fig. S8 and Table S3). The mass spectrometry data associated with this manuscript can be downloaded from ProteomeCommons.org Tranche using the following hash: p8qNGmu3/p6NkgODM4wlvXiiSkBQFit84XMsZJOl8Vk5vryUqCczF/OMpfvOwg8Y6gANmFHvc3korB8btN9BwWeeoNIAAAAAAAACiw==.

***In vitro* kinase assays.** For *in vitro* kinase assays, GFP immunoprecipitations were carried out from protein lysates from control (N2) or GFP::PAR-6-expressing embryos. The immunoprecipitations were incubated for 30 min at 25 °C with bacterially produced GST or GST–LIN-5 in kinase buffer containing 200 μM ATP, 50 mM HEPES at pH 7.5, 10 mM $MgCl_2$, 1 mM EGTA, 2 mM dithiothreitol and 20 μCi [γ-^{32}P]ATP for radioactive kinase assays. Reactions were terminated by the addition of SDS (5*x* sample buffer).

Antibodies and immunofluorescent staining. Phosphospecific antibodies against pS737 of LIN-5 were raised in rabbits against the peptide QRSSM-RpSESIQLASP, affinitiy purified against phosphopeptide and depleted of non-phospho-peptide reactivity with the non-phosphorylated peptide. For embryo stainings, gravid hermaphrodites were dissected in 10 μl of water on poly-(L-lysine)-

DOI: 10.1038/ncb2315

coated slides, freeze-cracked and fixed in a −20 °C methanol/acetone 1:1 mix for 10 min. Embryos were rehydrated in PBS and PBST (PBS containing 0.15% Tween-20), and blocked for 1 h at room temperature with 1% BSA and 10% donkey serum in PBST. All stainings with the pS737 antibody included the phosphatase inhibitor NaF at 50 mM in PBST. Primary antibodies were incubated overnight at 4 °C with either 1:300 rabbit anti-pS737, 1:500 mouse monoclonal anti-α-tubulin (Sigma, clone DM1A), 1:500 affinity-purified rabbit anti-GPR-1/2 (ref. 4), 1:50 mouse monoclonal anti-LIN-5 (refs 4,26) or 1:3 mouse monoclonal anti-P-granules K76. For staining with anti-pS737, unphosphorylated peptide QRSSMRSESIQLASP was added to the primary antibody mix at a final concentration of 1 μg ml^{-1} to sequester any unspecific antibody. Slides were washed three times with PBST and incubated for 45 min with 1:1,000 secondary antibodies, goat anti-rabbit Alexa Fluor 568, goat anti-mouse Alexa Fluor 568, goat anti-rabbit Alexa Fluor 488 or goat anti-mouse Alexa Fluor 488 (Invitrogen). Slides were washed three times, stained with DAPI and mounted in ProLong Antifade Gold (Invitrogen).

Quantification of cortical staining. To quantify cortical and cytoplasmic fluorescence intensities of LIN-5 and LIN-5 pS737 staining, confocal images were taken of one-cell stage embryos in the plane in which both spindle poles were in focus. Using ImageJ software, cortical fluorescence intensities were obtained by taking 30 line scans perpendicular to the cortex, and averaging 15 line scans on the anterior cortex and 15 line scans on the posterior cortex. Cytoplasmic fluorescence intensities were determined by taking 14 line scans just below and parallel to the cortex, along the whole cortex. Embryos were grouped into three different stages: prometaphase/metaphase (condensed DNA that is aligned or in the process of aligning at the metaphase plate; nuclear envelope not visible), anaphase (based on the extent of chromosome separation) and telophase (based on the extent of chromosome separation, decondensation of the DNA and flattening of the posterior spindle pole). By titration of the amount of antibody used, and by taking thin confocal images, we were able to detect asymmetries in LIN-5 localization that were previously not observed[4].

Live-cell imaging and quantification of spindle positioning. For the functional analysis of wild-type and phospho-mutant LIN-5, dsRNA corresponding to the first 377 nucleotides of *lin-5* messenger RNA was generated and injected into N2, *Ppie-1::LIN-5* (strains SV1086 or SV1087), *Ppie-1::LIN-5 4A* (strains SV1088, SV1089, SV1090 or SV1091) and *Ppie-1::LIN-5 4E* (strains SV1092, SV1150 and SV1151) young adults. The phenotypes were confirmed in 2–4 individual lines, and the quantifications were carried out with the underlined strains. As the LIN-5 4A mutant showed the strongest phenotype at 25 °C, whereas the LIN-5 4E mutant showed the strongest phenotype at 15 °C, experiments were carried out at either 15 °C or 25 °C, and were compared with the wild-type control at the same temperature. For experiments at 15 °C, N2, *Ppie-1::LIN-5* and *Ppie-1::LIN-5 4E* young adults were injected with *lin-5* (377 nucleotides) dsRNA, and were kept at 15 °C for 48 h before live-cell imaging. For experiments at 25 °C, N2, *Ppie-1::LIN-5* and *Ppie-1::LIN-5 4A* young adults were injected with *lin-5* (377 nucleotides) dsRNA, and were kept at 25 °C for 30 h before live-cell imaging. In both cases, uninjected N2 controls were grown for the same period of time at the appropriate temperature. For live-cell imaging, adults were dissected in egg buffer on a poly-L-lysine-coated coverslip, and were filmed in a hanging drop, to avoid any spindle-positioning effects due to pressure on the embryo. Differential interference contrast (DIC) images were recorded of embryos from pronuclear meeting until completion of the first division at 5 s intervals with a ×100 1.4 numerical aperture PlanApochromat objective lens on a Zeiss Axioplan microscope. Images were analysed and quantified using AxioVision Rel 4.7 and ImageJ. The data quantifications for the pronuclear centration in Fig. 4a were obtained at 25 °C, except for the *Ppie-1::LIN-5 4E* embryos, which were obtained at 15 °C. The data quantifications for the spindle positioning in Fig. 4b were obtained at 15 °C, except for the *Ppie-1::LIN-5 4A* embryos, which were obtained at 25 °C. The control, non-injected N2, *lin-5*-dsRNA-injected N2 and *lin-5*-dsRNA-injected *Ppie-1::LIN-5* embryos showed no difference in centration or spindle positioning at the different temperatures. For centrosome tracking, individual centrosomes were manually tracked using the Manual Tracking plugin from ImageJ.

Spindle severing. Experiments were carried out similarly to previous studies[14] using a spinning-disc confocal microscope equipped with a laser ablation system. For laser ablation, a 10 μm × 10 μm plane was ablated using a diode-pumped solid-state laser on 100 equally spaced points, each shot at 30 Hz. Images of GFP–tubulin were taken at 0.5 s intervals and the position of the spindle poles was automatically tracked using the MTrack2 plugin in Fiji (ImageJ). Peak velocities of the anterior and posterior spindle poles were determined within a 10 s time frame after ablation. For analysis of spindle pulling forces in LIN-5 wild type, LIN-5 4A and LIN-5 4E mutants, SV1143, SV1144 and SV1227 strains were injected with *lin-5* (377 nucleotides) dsRNA and kept at 25 °C for 24 h (SV1143, SV1144) or at 16 °C for 48 h (SV1143, SV1227) before ablations. The LIN-5 wild-type strain SV1143 showed no difference in spindle pole peak velocities when grown at 15 °C or 25 °C. All imaging and spindle ablations were carried out at room temperature.

Yeast two-hybrid analysis of LIN-5–GPR-1 interaction. DB::GPR-1- and AD::LIN-5-encoding plasmids were transformed sequentially into yeast strain Y8930 (ref. 32). Positive interactions were identified on the basis of the activation of the HIS3 and ADE2 reporter genes, indicated by growth on Sc (synthetic complete) −Leu−Trp −His and Sc −Leu −Trp−Ade plates.

32. Boxem, M. *et al.* A protein domain-based interactome network for *C. elegans* early embryogenesis. *Cell* **134,** 534–545 (2008).
33. Vidal, M. *et al.* Reverse two-hybrid and one-hybrid systems to detect dissociation of protein–protein and DNA-protein interactions. *Proc. Natl Acad. Sci. USA* **93,** 10315–10320 (1996).
34. Fisk Green, R. *et al.* Identification of critical domains and putative partners for the *Caenorhabditis elegans* spindle component LIN-5. *Mol. Genet. Genom.* **271,** 532–544 (2004).
35. Golden, A. *et al.* Metaphase to anaphase (mat) transition-defective mutants in *Caenorhabditis elegans*. *J. Cell Biol.* **151,** 1469–1482 (2000).
36. Anderson, D. C., Gill, J. S., Cinalli, R. M. & Nance, J. Polarization of the *C. elegans* embryo by RhoGAP-mediated exclusion of PAR-6 from cell contacts. *Science* **320,** 1771–1774 (2008).
37. Pinkse, M. W. *et al.* Highly robust, automated, and sensitive online TiO_2-based phosphoproteomics applied to study endogenous phosphorylation in *Drosophila melanogaster*. *J. Proteome Res.* **7,** 687–697 (2008).
38. Cox, J. & Mann, M. MaxQuant enables high peptide identification rates, individualized p.p.b.-range mass accuracies and proteome-wide protein quantification. *Nat. Biotechnol.* **26,** 1367–1372 (2008).
39. Olsen, J. V. *et al.* Global, *in vivo*, and site-specific phosphorylation dynamics in signaling networks. *Cell* **127,** 635–648 (2006).
40. Gouw, J. W. *et al.* *In vivo* stable isotope labeling of fruit flies reveals post-transcriptional regulation in the maternal-to-zygotic transition. *Mol. Cell Proteom.* **8,** 1566–1578 (2009).